4-1-2002

Mathematical Modeling and Computer Simulation of the Rotating Impeller Particle Flotation Process: Part II. Particle Agglomeration and Flotation

Mohammed D. Maniruzzaman

Makhlouf M. Makhlouf
Worcester Polytechnic Institute, mmm@wpi.edu

Mathematical Modeling and Computer Simulation of the Rotating Impeller Particle Flotation Process: Part II. Particle Agglomeration and Flotation

M. MANIRUZZAMAN and M. MAKHLOUF

Effective removal of unwanted particles from a molten metal alloy by flotation relies on purging a gas into the melt through a rotating impeller. This device is commonly known as a rotary degasser. Unwanted particles in the melt attach to the rising gas bubbles and rise to the slag layer where they are removed from the metal bulk. In addition, the turbulence created by the rotating impeller causes the randomly distributed solid particles to agglomerate into relatively large clusters. These clusters float up or settle down due to the difference between their density and that of the melt. A mathematical model has been developed to describe the particle dynamics and particle agglomeration that occur during the rotary degassing of aluminum melts. While previous investigations addressed particle collisions in low intensity turbulent fields where the size of the colliding particles is smaller than the Kolmogorov length scale, this model is more encompassing as it considers both low intensity and high intensity turbulence. Consequently, this model is more representative of a typical industrial rotary degassing operation.

I. INTRODUCTION

THE quality of molten metal can be improved by proper control of "unwanted phases" and impurities. In this context, the term unwanted phases refers to exogenous solid particles and/or liquid phases present above the liquidus temperature of the alloy as well as any gaseous phases dissolved in the melt. Among the various unwanted phases, solid particles and films have the most detrimental effect on a metal's properties. Consequently, various melt treatment techniques have been developed and are employed to remove solid particles and films from molten alloys.[1] Particle flotation using a rotary degasser, also known as fluxing, is one of the most widely used techniques for removing unwanted phases from molten alloys. In this process, a reactive or inert gas, or a combination of both types of gases is purged through a rotating impeller into the liquid metal. The most commonly used reactive gases are chlorine and fluorine, and the most commonly used inert gases are argon and nitrogen. While the gas, in the form of bubbles, rises to the surface, it encounters the particles and carries them to the top slag.[2] The efficiency of particle removal depends on the interaction between the bubbles and the particles. This interaction largely depends on the flow field inside the melt created by the flow of the bubbles as well as the impeller rotation and the size and number of bubbles. Particle removal also depends on the agglomeration of the particles caused by turbulence in the flow field.[3,4,5] The velocity and turbulence fields govern the transport of particles to the bubbles' surfaces. The addition of chlorine or other halogens affects the surface tension of the bubbles in such a way as to make the particles stick to the bubbles' surfaces more efficiently.[6–9] Figure 1 shows a schematic diagram of a rotary degasser.

A useful way of mathematically describing the dynamics of particle agglomeration in a rotary degasser is by means of a particle population balance. Although the mathematical formulation of the population balance is rather simple, it cannot be solved analytically to yield the particle size distribution. Moreover, a straightforward numerical approach to the problem puts practically prohibitive demands on computer time and memory. In this study, a mathematical model is presented to describe the agglomeration and removal of solid particles of varying sizes from an alloy melt during rotary degassing. A particle population balance is used to describe the system mathematically, and a special discretization scheme is employed to reduce the computational complexity and computer time required for solving the population balance equation. The model is used to investigate the effect of the rotary degasser's operational parameters on particle agglomeration and removal from a molten metal bath. This model is useful in the design of efficient rotary degassers and in selecting the operation parameters for optimum degasser performance.

II. THEORETICAL BACKGROUND

The state of a suspension of particles in a fluid may be conveniently described by a particle size distribution density function, $n_v(v, t)$, where $n_v(v, t)\,dv$ is the number of particles with volumes in the range v to $(v + dv)$ per unit volume of fluid. The dynamics of such a system in which individual particles may grow in size by accretion of mass from the fluid phase or shrink by loss of mass, and in which particles may collide and coagulate, is described by the general population balance equation (Reference 10)

M. MANIRUZZAMAN, Postdoctoral Fellow, and M. MAKHLOUF, Associate Professor, are with the Materials Science and Engineering Department, Worcester Polytechnic Institute, Worcester, MA 01609.

Manuscript submitted May 11, 2000.

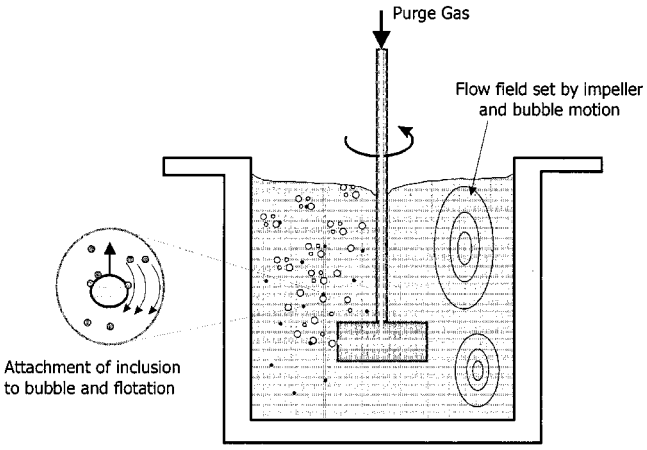

Fig. 1—Flotation treatment process using a rotary degasser.

$$\frac{\partial n_\nu(\nu, t)}{\partial t} = -\frac{\partial}{\partial \nu}[I_\nu(\nu, t) n_\nu(\nu, t)] + \int_0^{\nu/2} W_\nu(\nu - \tilde{\nu}, \tilde{\nu}) n_\nu(\nu - \tilde{\nu}, t) n_\nu(\tilde{\nu}, t)\, d\tilde{\nu} - n_\nu(\nu, t) \int_0^{\infty} W_\nu(\nu, \tilde{\nu}) n_\nu(\tilde{\nu}, t)\, d\tilde{\nu} + S_\nu[n_\nu(\nu, t), \nu, t] \quad [1]$$

where, $I_\nu(\upsilon, t) = d\upsilon/dt$, the rate of change of the volume of a particle of volume, υ, by transfer of material between the particle and the fluid phase, $W_\nu(\nu, \tilde{\nu})$ is the rate of collision between particles of volumes υ, and $\tilde{\nu}$, and S_υ is the net rate of addition of new particles into the system. The first term on the righthand side of Eq. [1] represents the rate of growth of particles by transfer of material to individual particles. The second term represents the rate of accumulation of particles in the size range $(\upsilon, \upsilon + d\upsilon)$ by collision of two particles of volume $(\nu - \tilde{\nu})$ and $\tilde{\nu}$ to form a particle of volume, υ, (assuming conservation of volume during coagulation). The third term represents the rate of loss of particles in the size range $(\upsilon, \upsilon + d\upsilon)$ by collision with all other particles. The last term represents all possible particle sources and sinks.

A number of approximation techniques for solving the population balance equation exist.[11,12,13] These include (a) defining the particle size distribution with a continuous function, (b) approximating the particle size distribution with a parameterized lognormal function, (c) describing the particle size distribution function by using moments of the particle size distribution function, and (d) discretizing the population balance equation. Method (a) was shown to be very accurate but requires a large amount of computer time.[12] Method (b) was demonstrated to be extremely fast but is limited in accuracy.[12] Method (c) is also limited in accuracy because it yields only the average properties of the particle size distribution. However, the loss of accuracy and resolution due to averaging is compensated for by an increase in computational speed and a reduction in computer memory requirements.[11] Method (d), in which the continuous particle size distribution is approximated by a finite number of sections with the properties within each section averaged, usually requires a large number of sections in order to achieve satisfactory accuracy and, therefore, is computer intensive.[11,12]

The solution of Eq. [1], by use of a conventional finite difference technique, is also very difficult because of the complex integral terms involved. To overcome this difficulty, the continuous population balance equation is replaced by a set of discretized equations.[4,14] For spherical particles, where the particle's volume is a function of the third power of the particle's radius, the discretized equations can be expressed in terms of the particle radius. Accordingly, the discretized equations for the rate of change in concentration of particles with average radius, r_k, in the kth size range (n_k) is given by

$$\frac{dn_k}{dt} = \frac{1}{2} \sum_{\substack{i=1 \\ i+j=k}}^{i=k-1} n_i n_j W(r_i, r_j) - \sum_{i=1}^{\infty} n_i n_k W(r_i, r_k) - S_k(n_k) \quad (k = 1, 2, \ldots, \infty) \quad [2]$$

In Eq. [2], $W(r_i, r_j)$ is the rate of collision between particles of radii r_i and r_j where the condition $\mathbf{r}_i^3 + \mathbf{r}_j^3 = r_k^3$ must always be satisfied. The first term on the right-hand side of Eq. [2] represents mass generation through collision and coagulation between the ith and jth particles, and the second term represents mass destruction through collisions of the kth particle with other particles. The last term, S_k, is the sink term that describes the rate of removal of particles by flotation. This flotation can be due to the density difference between the particles and the melt, as well as due to particle adhesion to the rising gas bubbles. Terms appearing in Eq. [2] will be described in detail in subsequent sections.

In order to solve Eq. [2], the size domain is divided into intervals of equal size ranges. This method gives greater numerical stability but usually requires a very large number of intervals. For example, to remove particles of the size range 1 to 40 μm with constant volume intervals assuming that the first interval spans the particle size range from 1 to 2^3 μm^3, a total of $\frac{40^3 - 1^3}{2^3 - 1^3} = 9143$ particle size intervals are required. If a smaller, more manageable number of size intervals is maintained in the discretization scheme, virtually no information will be conveyed about the smaller size particles.

III. THE MATHEMATICAL MODEL

The number of particle size intervals in a relatively wide size range can be reduced considerably without sacrificing information about the smaller size particles by employing a geometric series instead of a constant size interval. Indeed, if the series is geometric in length, it is also geometric in volume. Hunslow's method,[15] which is based on binary interaction mechanisms, is employed. In this method, the wide particle size domain over which particle agglomeration occurs is divided into intervals. Within each of these intervals, equations describing the change in particle concentration are used. Each interval is represented by a characteristic volume, V_k, that is the average volume of the particle sizes in the interval

$$V_k = \frac{b_{k-1} + b_k}{2} \quad [3]$$

where b_k is the upper boundary volume of interval k. V_k is

Table I. Binary Interaction Mechanisms That Are Necessary to Fully Describe Particle Agglomeration in a Flow Field

Mechanism Number	Birth or Death in Interval i	Collision between Particles in Intervals	
1	birth	$i-1$	$1 \rightarrow i-2$
2	birth	$i-1$	$i-1$
3	death	i	$i \rightarrow i-1$
4	death	i	$i \rightarrow \infty$

related to the previous interval V_{k-1} by a geometric series relationship such that, $V_k/V_{k-1} = 2$. In terms of length-domain discretization, $r_k/r_{k-1} = \sqrt[3]{2}$. This discretization scheme allows covering a great range of particle sizes in a manageable manner.

Four binary interaction mechanisms are necessary to fully describe particle agglomeration in a flow field. These are listed in Table I.

The particle size distribution is discretized in such a way that any interval of volume, ϑ_i, is twice the width of the previous interval, v_{i-1}, and the density function in the interval i is given by $n' = N_i/\nu_i$. N_i is the total number of particles in the interval i. It is convenient to assign the lower bound on interval i, a size (*i.e.*, volume) 2^i and the upper bound a size 2^{i+1}. The density function in this interval is, therefore, $n = N_i/2^i$. A detailed mathematical formulation for the rate of birth and the rate of death for the different mechanisms shown in Table I can be found in Reference 15.

(1) *Mechanism 1*. Birth in the ith interval can occur only when a particle in the $i-1$th interval agglomerates with a particle in the 1st to $i-1$th intervals. Consider the agglomeration of a particle of size, a, in the jth interval, where $j < i-1$. In order to form a particle in the ith interval it must collide with particles in the size range $2^i - a \le v < 2^i$, all of which are in the $i-1$th interval. The number of particles available for collision is, thus, $aN_{i-1}/2^{i-1}$. The rate of birth by mechanism 1 is

$$R_{i,j}^{[1]} = W_{i-1,j} \int_{2^j}^{2^{j+1}} a 2^{1-i-j} N_{i-1} N_j \, da = 3 \cdot 2^{j-i} W_{i-1,j} N_{i-1} N_j$$

If this rate is summed over all possible values of j, the total rate of birth in the ith interval by the first mechanism may be determined from

$$R_{i,j}^{[1]} = \sum_{j=1}^{i-2} 3 \cdot 2^{j-i} W_{i-1,j} N_{i-1} N_j \qquad [4]$$

(2) *Mechanism 2*. A similar process may be used to describe agglomerates formed in the ith interval by collision between particles both in the $i-1$th interval. The rate of birth is

$$R_i^{[2]} = W_{i-1,i-1} \int_{2^{i-1}}^{2^i} \frac{N_{i-1}^2}{2^i} \, da = \frac{1}{2} W_{i-1,i-1} N_{i-1}^2 \qquad [5]$$

The leading factor of one-half is included to avoid counting collisions twice.

(3) *Mechanism 3*. Death by agglomeration will occur to a particle in the ith interval should it collide and adhere to a particle of sufficient size for the resultant agglomerate to be larger than the upper size limit of the ith interval. First, consider collisions with particles from smaller size ranges. Death in the ith interval will occur when a particle of size a, in the jth interval, agglomerates with a particle ranging in size from $2^{i+1} - a$ to 2^{i+1}. The number of particles in this latter range is $aN_i/2^i$. The rates may be calculated as before

$$R_{i,j}^{[3]} = 3 \cdot 2^{j-i-1} W_{i,j} N_i N_j$$

By summing this last equation over all possible values of j, death by the third mechanism may be represented by

$$R_i^{[3]} = N_i \sum_{j=1}^{i-1} 3 \cdot W_{i,j} \, 2^{j-i-1} N_j \qquad [6]$$

(4) *Mechanism 4*. If a particle in the ith interval agglomerates with a particle from that or higher interval, a death occurs in the ith interval. This final mechanism may be given by

$$R_i^{[4]} = N_i \sum_{j=1}^{\infty} W_{i,j} N_j \qquad [7]$$

The overall rate of change of number of particles (dN_i/dt) may be computed by combining Eqs. [4] through [7], *i.e.*,

$$\frac{dN_i}{dt} = CR_i^{[1]} + R_i^{[2]} - CR_i^{[3]} - R_i^{[4]} \qquad [8]$$

The term C in Eq. [8] is a volume correction factor. It is shown[15] that in order to conserve particle volume, the value of C should be 2/3.

Equation [9] is the expanded form of Eq. [8].

$$\frac{dN_i}{dt} = N_{i-1} \sum_{j=1}^{i-1} 2^{j-i+1} W_{i-1,j} N_j + \frac{1}{2} W_{i-1,i-1} N_{i-1}^2 - N_i \sum_{j=1}^{i-1} 2^{j-i} W_{i,j} N_j - N_i \sum_{j=i}^{\infty} W_{i,j} N_j \qquad [9]$$

Finally, a "sink" term (S_k) is introduced into Eq. [9] to account for particle removal from the system.

$$\frac{dN_k}{dt} = \sum_{i=1}^{i=k-2} 2^{i-k+1} N_{k-1} N_i W(r_{k-1}, r_i) + \frac{1}{2} N_{k-1}^2 W(r_{k-1}, r_{k-1}) - \sum_{i=1}^{k-1} 2^{i-k} N_i N_k W(r_i, r_k) - \sum_{i=k}^{\infty} N_i N_k W(r_i, r_k) - S_k N_k \qquad [10]$$

A. *Determination of the Particle Agglomeration Rate, $W(r_i, r_j)$*

Particle agglomeration in a flotation melt treatment process is the consequence of collision between particles. The

collision mechanism largely depends on the type of flow, *i.e.*, on the hydrodynamics of the melt and the size of the particles. Several agglomeration mechanisms are possible. These include Brownian agglomeration, which is more active in submicron size particles; gravitational agglomeration, which is typical of very large particles; and turbulent agglomeration, which is typical of intermediate size particles. In typical rotary degassers, the melt hydrodynamics is such that only turbulent agglomeration is relevant. Consequently, Brownian and gravitational agglomeration mechanisms are excluded from the model. During rotary degassing of molten metals, mechanical energy is supplied to the melt by the rotation of the degasser's impeller and by the flow of the purged gas. This energy creates turbulence within the melt. The turbulence creates eddies, which in turn help dissipate the energy. The energy is transferred from the largest eddies to the smallest eddies in which it is dissipated through viscous interactions. The size of these smallest eddies is the Kolmogorov microscale, η, which is expressed as a function of the kinematic viscosity, ν, and the energy dissipation rate, ε,

$$\eta = \left(\frac{\nu^3}{\varepsilon}\right)^{1/4} \qquad [11]$$

The rate of particle agglomeration, $W(r_i, r_j)$, consists of two components,[14]

$$W(r_i, r_j) = W_t + W_s \qquad [12]$$

where W_t is the collision rate of particles caused by turbulence eddies, and W_s is the rate of collisions caused by the difference in flotation velocity between large and small particles, known as Stokes collisions.

In the turbulent flow field, agglomeration can occur by either of two mechanisms. The first mechanism, which will be referred to as the *viscous subrange mechanism*, is active when the particles are smaller than the Kolmogorov microscale, η. In this case, agglomeration is assumed to take place under local shear flow conditions.[4,5,16] The second mechanism, which will be referred to as the *inertial subrange mechanism*, is active when the particles are larger than the Kolmogorov microscale, η. In this case, the colliding particles assume independent velocities. The model presented here incorporates both turbulent flow mechanisms—the *viscous subrange mechanism* and the *inertial subrange mechanism*—since in a rotary degasser the turbulence intensity is quite high and the particle size distribution is such that it may satisfy the requirements of both mechanisms. A parameter, β_1, is used to determine which agglomeration mechanism is dominant in a given turbulent flow field. The parameter, β_1, is defined as the ratio of the particle size to the Kolmogorov microscale, η. When $\beta_1 < 1$, the viscous subrange mechanism is dominant; on the other hand, when $\beta_1 > 1$, the inertial subrange mechanism is dominant.

For $\beta_1 < 1$, the approach velocity of the colliding particles is determined by their motion within the eddy. Therefore, particle collisions are influenced by the local shear within the eddy. Based on work by Saffman and Turner,[17] the rate of collision between two particles of size ranges r_i and r_j in the viscous subrange region can be described by Eq. [13]

$$W_t(r_i, r_j) = 1.30\ \alpha_T (r_i + r_j)^3 \left(\frac{\varepsilon}{\nu}\right)^{0.5} \Delta \qquad [13]$$

In Eq. [13], ε is the turbulence dissipation rate, and ν is the kinematic viscosity of the melt. The term Δ is a correction coefficient that is introduced to account for any turbulence heterogeneity that may be present in the treatment reactor.*

*For example, heterogeneity may be introduced when a noncylindrical impeller is used.

The empirical capture efficiency coefficient of collision, α_T, describes the hydrodynamic and attractive interactions between agglomerating particles. Higashitani *et al.*[4] suggested the following relationship for evaluating α_T.

$$\alpha_T = 0.732 \left(\frac{5}{N_T}\right)^{0.242} \quad ; \quad N_T \geq 5 \qquad [14]$$

where N_T is the ratio between the viscous force and the Van der Waals force,

$$N_T = \frac{6\pi\mu(r_i + r_j)^3 \dot{\gamma}}{A} \qquad [15]$$

In Eq. [15], A is the Hamaker constant, and $\dot{\gamma}$ is the fluid deformation rate,

$$\dot{\gamma} = \left(\frac{4\varepsilon}{15\pi\nu}\right)^{0.5}$$

On the other hand, for $\beta_1 < 1$, the particles are larger than the smallest eddy; consequently, they are dragged by velocity fluctuations in the flow field and collide with one another. In this case, the rate of collision is expressed using Abrahamson's model.[18] Abrahamson assumed 100 pct collision efficiency. In the model presented here, Abrahamson's equation is modified by a capture efficiency coefficient, α_T, which accounts for attractive and hydrodynamic interactions between particles:

$$W_i(r_i, r_j) = 5\alpha_T (r_i + r_j)^2 \sqrt{(\overline{U}_i^2 + \overline{U}_j^2)} \qquad [16]$$

where $\overline{U}_i^2$ is the mean squared velocity for particle i. When the flow is highly turbulent and the particles are relatively large in comparison to the smallest eddy, which is the case in typical rotary degassing of molten metals, the particles acquire momentum from the eddies and are projected into neighboring eddies without necessarily following the fluid fluctuations. In this case, the mean squared velocity is calculated using Eq. [17].[18]

$$\overline{U}_i^2 = \frac{\overline{U}^2}{1 + 1.5\tau_p \varepsilon / \overline{U}^2} \qquad [17]$$

where, $\overline{U}^2$ is the mean squared velocity deviation of the fluid, and τ_p is the relaxation time of a particle of radius r_p ($\tau_p = 2\rho_p r_p / 18\mu$). Equation [17] is applicable only when one of the colliding particles has a radius

$$r = \sqrt{(15\mu\overline{U}^2)/(4\rho_{\text{particle}}\varepsilon)} \qquad [18]$$

When the particles are smaller than the limiting size given by Eq. [18], they are not completely influenced by the eddies, and Eq. [19] instead of Eq. [17] is used to calculate the mean squared particle velocity, $\overline{U}^2$,[19]

$$\overline{U}_i^2 = \frac{4a^2}{(2a + 3)^2} (\varepsilon\nu)^{1/2} \frac{3}{\delta(\delta + 1)} \qquad [19]$$

where $a = (\rho_{\text{particle}} - \rho_{\text{melt}})/\rho_{\text{melt}}$ and $\delta = (9\rho_{\text{melt}}/2\rho_{\text{particle}} + \rho_{\text{melt}})(\eta/r_i)^2$

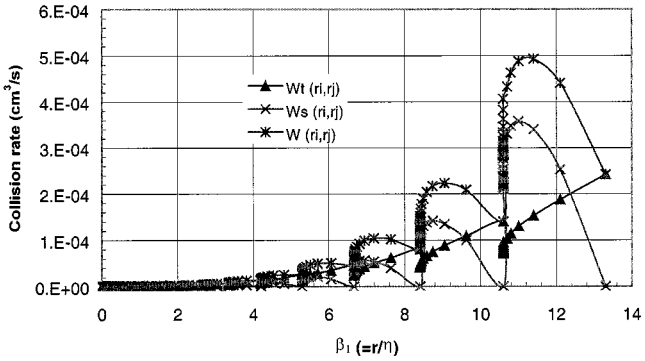

Fig. 2—Variation of particle collision rate with particle size in a rotary degasser operating at 675 rpm with a gas flow rate of 36 L of argon per minute.

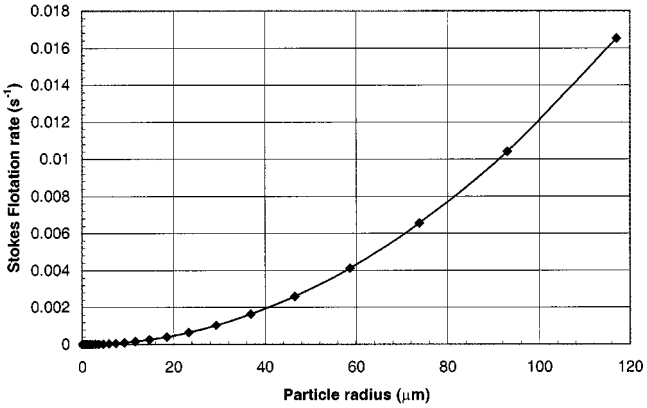

Fig. 3—Variation of Stokes flotation rate with particle size in a typical rotary degasser.

The Stoke collision rate, W_S, is calculated from Eq. [20]:[20]

$$W_s = \frac{2\pi\Delta\rho g}{9\mu}(r_i + r_j)^3|r_i - r_j| \qquad [20]$$

where $\Delta\rho$ is the difference in density between the particles and the melt.

Figure 2 shows the particle agglomeration rate as a function of β_1 after 10 minutes of degassing in a rotary degasser that is operating at 675 rpm with a flow rate of 36 L of argon gas per minute. These operation parameters result in a turbulence dissipation rate $\varepsilon = 23.09\ m^2/s^3$.[18] The turbulent collision rate, W_t is calculated from Eq. [13] and [16], and the Stokes collision rate, W_s, is calculated from Eq. [20]. Figure 2 shows that for a particular size class, r_k, both W_t and W_s increase as the radii of the colliding particles increase, but as the radius of one of the colliding particles approaches that of the other, W_s begins to decrease and approaches zero as the particle radii become equal. Due to the combined effect of W_t and W_s, W within a particular particle size interval initially increases and then rapidly decreases.

B. *Determination of the Particle Flotation Rate, S_k*

Removal of particles from the melt by flotation, represented by S_k in Eq. [10], is due to Stokes flotation and settling of relatively large particles, S_s, and attachment of particles to the rising gas bubbles, S_b.

$$S_k = S_s + S_b \qquad [21]$$

Assuming Stokes terminal velocity and a homogeneous distribution of particles in the melt, the Stokes flotation rate for particles of size class k is calculated using Eq. [22]:[14]

$$S_s = \frac{2g}{9\mu L}\Delta\rho r_k^2 \qquad [22]$$

In Eq. [22], L is the depth of molten metal in the reactor, g is gravitational acceleration, μ is viscosity of the molten metal, and $\Delta\rho$ is the difference in density between the solid particles and the melt. Figure 3 shows a typical Stokes' flotation curve. The larger the particle size, the higher the flotation rate is.

The rate of attachment of particles to the gas bubbles, S_b, is calculated assuming the particles' centerlines flow along streamlines and that attachment to the bubbles occurs whenever the streamline carrying the particle comes within a distance that is smaller in magnitude than the particle's radius.[14] Assuming that the particles are distributed homogeneously within the melt, the entrapment rate of particles of size class k on gas bubbles is given by Eq. [23]:[14,21]

$$S_b = \frac{N_b \upsilon_b b_k^2 \pi}{V} \qquad [23]$$

In Eq. [23], N_b is the number of bubbles, υ_b is the velocity difference between the bubbles and the melt, V is the volume of the melt, and b_k is the critical entrapment distance between bubbles and particles of size class k. Equation [23] assumes that when the particles are within a volume $\upsilon_b b_k^2 \pi$, they instantaneously attach to the bubble. However, particle attachment to bubbles requires time, hence, S_b is modified by an entrapment efficiency, E, where $E = 4r_k/r_b$, and r_b is the average stable bubble radius,[2,22]

$$S_b = \frac{N_b \upsilon_b b_k^2 \pi}{V} E \qquad [24]$$

The terminal velocities of gas bubbles in molten metals are difficult to measure accurately. However, Szekely[2] proposed Eq. [25] based on measurements of the terminal velocity of gas bubbles in water.

$$\upsilon_b = \sqrt{\sigma We/2\rho r_b} \qquad [25]$$

In Eq. [25], ρ is the density of the melt, σ is the surface tension of the melt, and We is Weber's number. The number of bubbles in the reactor (N_b) is calculated from the volume fraction of the purged gas and the average stable bubble radius, r_b. The volume fraction of purged gas is estimated from numerical simulations of the flow field within the reactor,[23] and the average stable bubble radius in a turbulent flow field is estimated using Hinze's formula[24] with a modification applicable to a rotary degasser suggested by Johansen *et al.*,[25,26]

$$r_b = \frac{1}{2} D\left(\frac{Q_g}{Q_{go}}\right)^m \left(\frac{We_c\sigma}{\rho}\right)^{0.6} \frac{1}{\varepsilon^{0.4}} \qquad [26]$$

In Eq. [26], $Q_{go} = 25$ L/min, $D = 0.878$, $m = 0.28$ (assuming a cylindrical impeller), and Q_g is the gas flow rate in L/min. A critical Weber number, $We_c \approx 4$, is necessary for the bubble to be stable.[21]

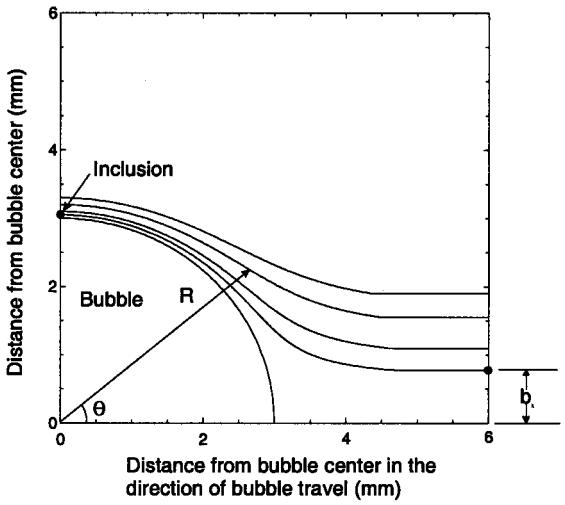

Fig. 4—Streamlines around a 6 mm diameter argon gas bubble based on the assumption of potential flow.

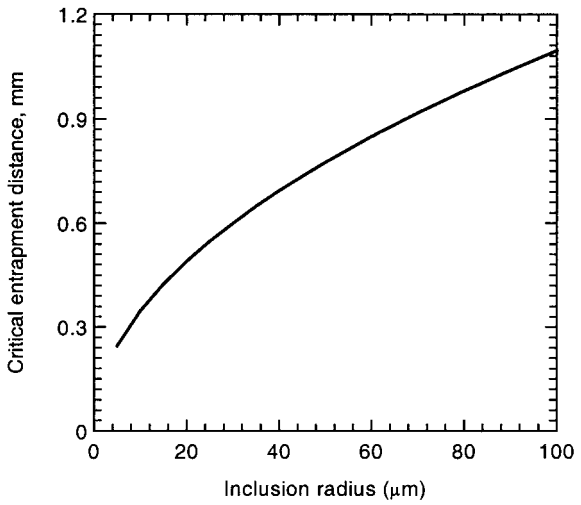

Fig. 5—Critical entrapment distance as a function of particle radius.

The streamlines around a gas bubble of radius, r_b, shown in Figure 4, is calculated using Eq. [27], which assumes potential flow around the bubble[27]

$$\psi = \frac{1}{2}\, u_b r_b^2 \sin^2\theta \left(\frac{R^2}{r_b^2} - \frac{r_b}{R}\right) \qquad [27]$$

In Eq. [27] ψ is the stream function, and u_b is the bulk velocity. Equation [27] is used to back calculate the critical entrapment distance, b_k, as follows. First, Eq. [27] is rewritten in the form

$$\psi = u_b r_b^2 \sin^2\theta \left[\frac{1}{2}\, x^2 - \frac{1}{2x}\right] \qquad [28]$$

where $x = R/r_b$. When $\theta = 90$ deg, $R = r_p + r_b$, and, therefore, $x = x_E = 1 + r_p/r_b$. Recognizing that at a distance far removed from the bubble $\sin\theta = \dfrac{b_k}{R}$, and substituting into Eq. [28], b_k is expressed in terms of ψ and u_b,

$$\mathbf{b}_k^2 = \frac{2\psi}{\mathbf{u}_b} \qquad [29]$$

Figure 5 shows the critical entrapment distance for particles of radius varying between 5 and 100 μm by 6-mm diameter argon gas bubbles.

Figure 6 shows the variation in flotation rate due to particle attachment to bubbles, S_b, with particle radius. S_b is calculated using Eq. [24] and Figure 6 shows that S_b increases linearly with particle size. Figure 7 shows the variation of the product of flotation rate, S_k, and the number of particles in the size class k, N_k, with particle radius.

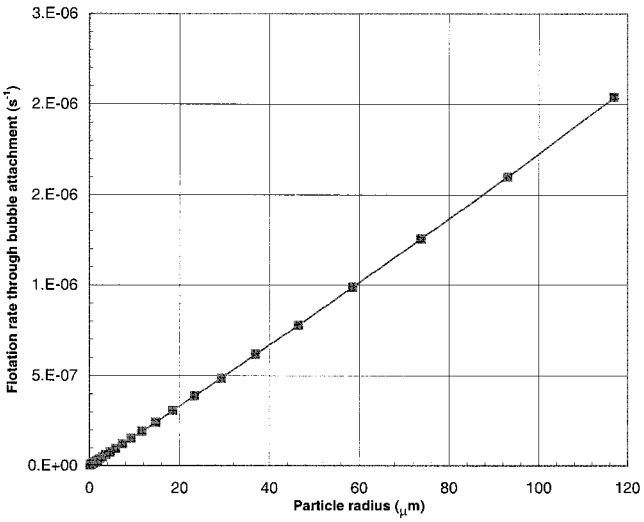

Fig. 6—Variation of the flotation rate due to bubble attachment with particle size.

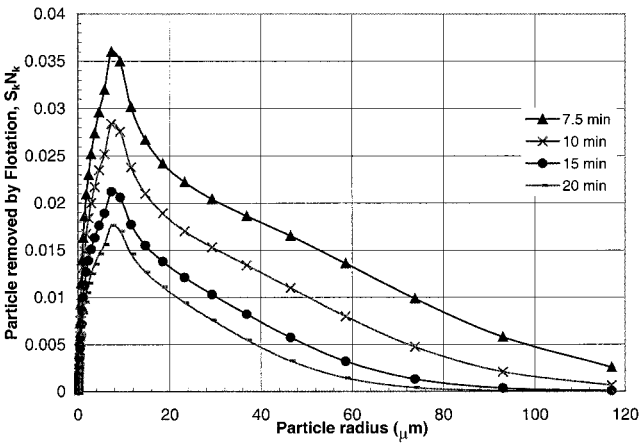

Fig. 7—Variation of S_kN_k, with particle size.

IV. VERIFICATION OF THE MODEL PREDICTIONS

In order to verify the model predictions, aluminum oxide powder of a known particle size distribution was introduced into commercially pure molten aluminum held at 750 °C in an electrical furnace. In order to facilitate incorporation of the powder into the molten aluminum, it was wrapped in a thin copper foil and upon introduction into the melt; the melt was gently stirred to enhance dissolution of the copper foil and mixing and distribution of the particles. The furnace

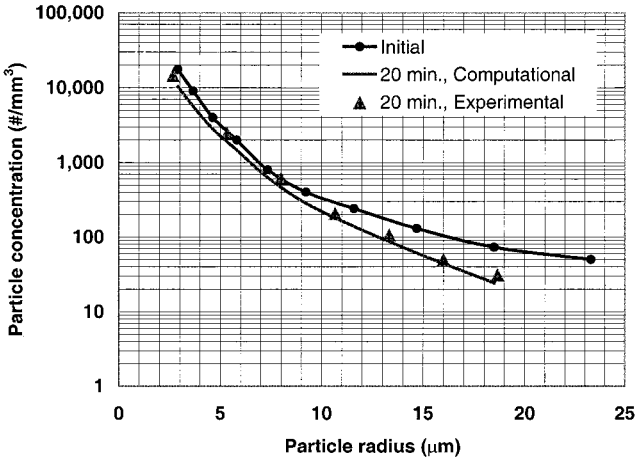

Fig. 8—Comparison between measured and model predicted particle concentration *vs* particle radius curves.

was 0.224 m in diameter and 0.45-m high, and the initial melt depth was 0.3 m. A laboratory size rotary degasser was used to purge high purity argon gas into the melt. The diameter of the degasser's rotor shaft was 24 mm, and the diameter of the cylindrical impeller was 80 mm. The gas was purged at a rate of 2 L/min through 12, 8-mm-diameter side holes that were equally spaced around the circumference of the impeller. The impeller was placed so that its bottom was 5 cm above the bottom of the furnace and was operated at 560 rpm. Maniruzzaman and Makhlouf[23,28] used computational fluid dynamics to simulate a similar reactor and obtained a mean turbulence energy dissipation rate of 0.333 m^2/s^3 and an argon gas volume fraction of 0.0725.

Samples were taken from the holding furnace using a covered sampling cup before and after purging with argon for 20 minutes. The solidified samples were sectioned, mounted in epoxy, and polished using standard metallographic procedures. The aluminum oxide particle size distribution in each sample was determined using image analysis.*

*AnalySIS 2.11 software is manufactured and marketed by Soft Imaging System GmbH (D-48153 Münster, Germany).

A minimum of 50 fields from each sample was examined at 350X magnification, and the particle count per unit area was converted to particle count per unit volume using standard stereological estimation techniques.[29] Figure 8 shows the measured initial particle concentration *vs* particle radius curve, as well as the measured particle concentration *vs* particle radius curve after 20 minutes of purging with argon. Also shown in Figure 8 is the computer predicted particle concentration *vs* particle radius curve after 20 minutes of purging. Figure 8 shows good agreement between the model predicted and the measured particle concentration profiles.

V. SIMULATION RESULTS AND DISCUSSION

The model was used to evaluate the change in aluminum oxide particle size distribution during treatment of molten aluminum in a rotary degasser. The evolution of the particle size distribution is simulated by solving the discretized population balance (Eq. [10]). The initial particle radius domain, which spans the range 0.05 to 120 μm, is discretized into

Table II. Rotary Degasser Operation Parameters Used in the Simulations and Their Corresponding Mean Turbulence Dissipation Rate (ε) and Volume Fraction of Bubbles (V_f)[18]

Case Number	Impeller Speed (rpm)	Rotation Direction	Gas Flow Rate (L/min)	ε (m^2/s^3)	V_f
1	675	unidirection	36	23.09	4.31
2	675	reverse rotation	36	31.51	4.60
3	350	reverse rotation	36	0.17	4.70
4	675	reverse rotation	15	26.43	3.97

Table III. Physical Properties and Data Used in the Simulations

Molten aluminum at 973 K	
Density	2300 kg/m^3
Viscosity	2900 Pa · s
Surface tension	0.9 N/m
Kinematic viscosity	1.3×10^{-6} m^2/s
Aluminum oxide particles at 973 K	
Density	3500 kg/m^3
Hamaker constant	0.45×10^{-20} J[14]

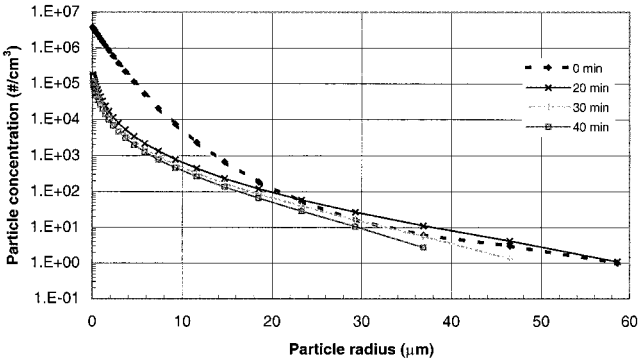

Fig. 9—Particle size distribution in a rotary degasser operating at 350 rpm, 36 L/min gas flow rate and periodic reversal of rotation direction.

35 sections each representing a particle radius range. The discretized ordinary differential equations system is solved using the explicit Euler method.

Two inputs are necessary for calculating the particle collision rate. These are the mean turbulence dissipation rate and the volume of purged gas. Maniruzzaman and Makhlouf[23] used computational fluid dynamics and calculated these parameters for a rotary degasser operating with the parameters shown in Table II.

Other physical data necessary for calculating the particle collision rate are shown in Table III.

Figure 9 shows the particle size distribution in a rotary degasser operating under the conditions of case 3 in Table II. Figure 9 shows that under these conditions the number of particles with radii smaller than 20 μm initially decreases rapidly. This rapid decrease in the number of small sized particles is due to their rapid rate of agglomeration into larger particles. Because the rate of agglomeration of particles with radii less than 20 μm into particles with radii larger than 20 μm exceeds the rate of removal of the large particles by

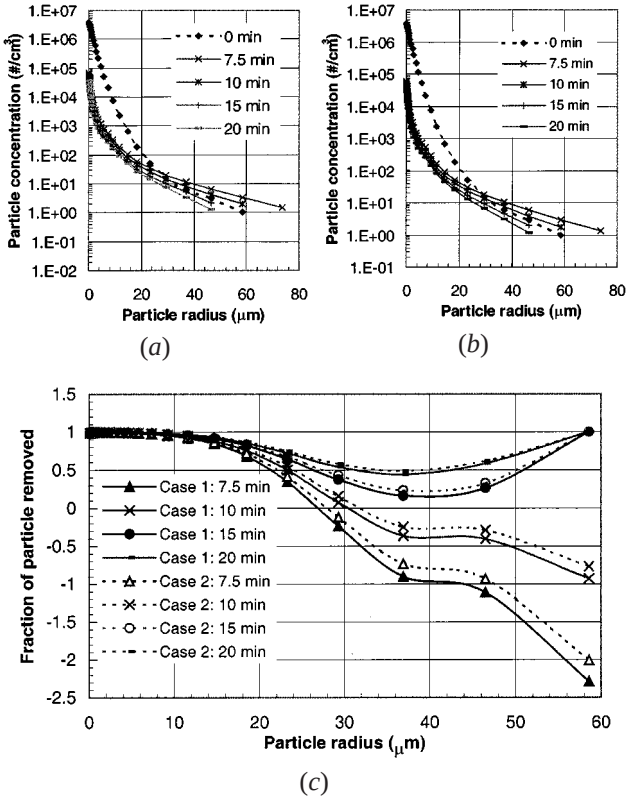

Fig. 10—Effect of rotation direction on particle size distribution in a rotary degasser. (*a*) Particle concentration profile for case 1, (*b*) particle concentration profile for case 2, and (*c*) particle removal efficiency.

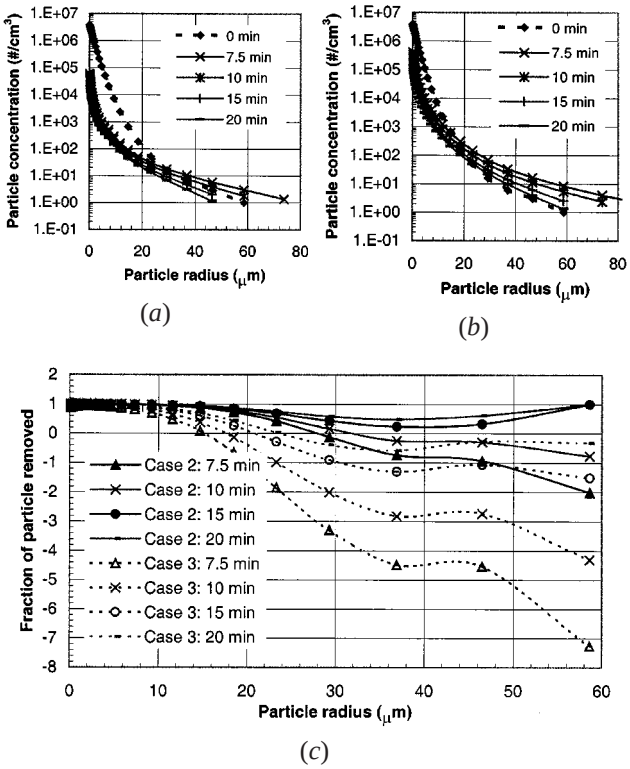

Fig. 11—Effect of rotation speed on particle size distribution in a rotary degasser. (*a*) Particle concentration profile for case 2, (*b*) particle profile for case 3, and (*c*) particle removal efficiency.

flotation, there is an initial net increase in the number of particles with radii larger than 20 μm. Only after degassing for more than 20 minutes does the rate of particle removal catch up with the rate of particle agglomeration, and an overall reduction in the number of particles occurs.*

*It should be noted that the critical particle radius for transition between the viscous subrange model and the transition subrange model is about 30 μm and between the transition subrange model and the inertial subrange model is about 815 μm.

Figure 10 shows the effect of reversing the direction of rotation in a rotary degasser on particle removal when the degasser is operating at a relatively high rotation speed and relatively high gas flow rate. Figures 10(a) and (b) show the variation in particle size distribution with time for cases 1 and 2 of Table II, respectively. In both cases, particles smaller than 25 μm agglomerate rapidly due to turbulent collisions. Removal of the large particles depends mainly on a combination of turbulent agglomeration, which leads to formation of even larger particles, and flotation by attachment to bubbles and Stokes' flotation. Although there is an accumulation of larger particles during the early stages of degassing, with time, the larger particles are removed. Figure 10(c) compares the particle removal efficiency of two similar degassers one operating under the conditions depicted in case 1 of Table II, the other under conditions depicted by case 2. The particle removal efficiency is calculated in terms of the fraction of particles removed from each particle size range normalized to the initial number of particles in the size range. The negative particle removal efficiency values indicate an increase in the number of particles of that size. Figure 10(c) shows that the efficiency of the degasser operating under the conditions depicted in case 2 of Table II is higher than that of the degasser operating under the conditions depicted in case 1 of Table II.

The particle removal efficiency *vs* particle size curve, shown in Figure 10(c), can be divided into three distinct regions. In region I, which includes particle sizes up to 15 μm, the dominant mechanism responsible for particle removal is turbulent agglomeration. The initial number of particles in this size range is very high; consequently, despite the high particle removal rate in this size range, many particles remain in the melt. In region II, which includes particles between 15 and 40 μm, the rate at which particles grow by turbulent agglomeration is not balanced by the rate of particle removal by flotation; consequently, particles in this size range are difficult to remove. In region III, which includes all particles larger than 40 μm, although there is continued formation of particles in this range by turbulent agglomeration of smaller particles, given time, this supply of particles is more than balanced by the high removal rate.

Figure 11 shows the effect of rotation speed on degasser performance. Figures 11(a) and (b) show the particle concentration profiles for cases 2 and 3 of Table II, respectively. Figures 11(a) and (b) show that the rate of particle removal is slow when the impeller rotation speed is low. Figure 11(c) compares the particle removal efficiency of two degassers one operating under the conditions depicted in case 2 of Table II, the other under the conditions depicted in case 3. Figure 11(c) shows that increasing the rotation speed greatly enhances particle removal. At the high rpm, particles with radii ranging between 25 and 40 μm are the most difficult to remove, while at the low rpm, the difficult to remove

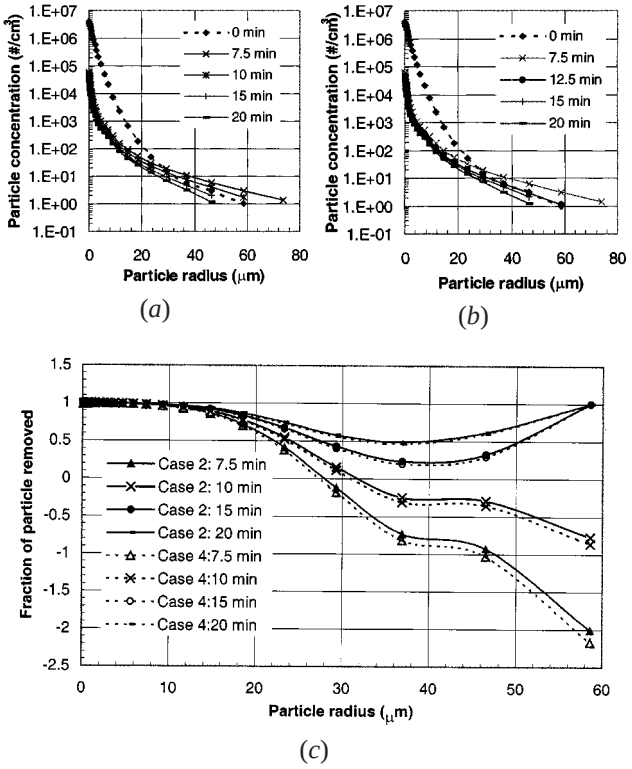

Fig. 12—Effects of gas flow rate on particle size distribution in a rotary degasser. (*a*) Particle concentration profile for case 2, (*b*) profile for case 4, and (*c*) particle removal efficiency.

particle size range includes all particles larger than 10 μm. Figure 9 shows that degassing for a relatively long time (more than 20 minutes) at the low rpm is necessary to remove these particles.

Figure 12 shows the effect of the purge gas flow rate on degasser performance. Figures 12(a) and (b) show the particle concentration profiles for cases 2 and 4 of Table II, respectively. The rate of particle removal is similar for both cases indicating that at high impeller rotation speeds, the gas flow rate does not have a very pronounced effect on the degasser's performance. Figure 12(c) compares the particle removal efficiency of two degassers, one operating under the conditions depicted in case 2 of Table II, the other under the conditions depicted in case 4. Figure 12(c) shows that increasing the purge gas flow rate enhances particle removal but only slightly.

VI. CONCLUSIONS

A model that describes particle collision and removal by flotation during rotary degassing of molten metals is developed. The model is based on the classical theory of turbulent agglomeration and is unique in that it accounts for both high and low intensity turbulent flow conditions. A particle population balance is used to describe the system mathematically, and a special discretization scheme is employed to reduce the computational complexity and the computer time required for solving the population balance equation. The model is used to investigate the effect of the rotary degasser's operational parameters on the agglomeration of aluminum oxide particles and their removal from molten aluminum. The model explains the interrelationships between the various mechanisms responsible for particle removal and is useful in the design and efficient operation of industrial rotary degassers.

NOTATIONS

A	Hamaker constant
a	particle radius
b_k	critical entrapment distance between bubbles and particles of size class k
b_k	upper boundary volume of interval k
C	volume correction factor
E	entrapment efficiency
g	acceleration of gravity
I_v	the rate of change of the volume of a particle
n, n'	density function
n_k	concentration of particles in the kth size range
n_v	particle size distribution density function
N_i	total number of particles in the interval i
N_T	ratio between the viscous force and the Van der Waals force
N_b	number of bubbles
Q_g	gas flow rate
r_b	average stable bubble radius
r_k	average radius of particle in the kth size range
R	rate of agglomeration
S_b	rate of attachment of particles to the rising gas bubbles
S_s	Stokes flotation and settling rate
S_k	rate of removal of particles by flotation
S_v	the net rate of addition of new particles into the system
t	time
u_b	bulk velocity of fluid
$\overline{U}^2$	mean squared velocity deviation of the fluid
$\overline{U}_i^2$	mean squared velocity for particle i
V	volume of the melt
$u, \tilde{v}$	unit volume of fluid
V_k	average volume of the particles in size interval k
v_b	velocity difference between the bubbles and the melt
We	Weber's number
W_v, W	rate of collision between particles
W_s	Stokes collisions rate
W_t	collision rate of particles caused by turbulence eddies
α_T	empirical capture efficiency coefficient of collision
β_1	ratio of the particle size to the Kolmogorov microscale
$\dot{\gamma}$	fluid deformation rate
τ_p	relaxation time of a particle
ρ	density
ψ	stream function
μ	viscosity of the molten metal
ε	energy dissipation rate
ν	kinematic viscosity of the melt
η	Kolmogorov microscale
σ	surface tension of the melt
Δ	correction coefficient

REFERENCES

1. M. Maniruzzaman and M.M. Makhlouf: *Phase Separation Technology in Aluminum Melt Treatment*, American Foundrymen's Society, Des Plains, IL, 2000.
2. A.G. Szekely: *Metall. Trans. B*, 1975, vol. 6B, pp. 259-70.
3. R. Gammelsæter, K. Bech, and S.T. Johansen: *Light Met.*, 1997, pp. 1007-11.
4. K. Higashitani, K. Yamauchi, Y. Matsuno, and G. Hosokawa: *J. Chem. Eng. Jpn.*, 1983, vol. 16, pp. 299-304.
5. K. Nakanishi and J. Szekely: *Trans. Iron Steel Inst. Jpn.*, 1975, vol. 15, pp. 522-30.
6. O. Hjelle, T.A. Engh, and B. Rasch: *International Seminar on Refining and Alloying of Liquid Aluminum and Ferro-Alloys*, Trondheim, Norway, 1985, pp. 345-60.
7. B. Kulunk and R. Guthrie: *Light Met.*, 1992, pp. 963-75.
8. G. Sigworth: *Light Met.*, 2000, pp. 773-78.
9. E.M. Williams, R.W. McCarthy, S.A. Levy, and G.K. Sigworth: *Light Met.*, 2000, pp. 785-93.
10. F. Gelbard and J.H. Seinfeld: *J. Comput. Phys.*, 1978, vol. 28, pp. 357-75.
11. J.D. Landgrebe and S.E. Pratsinis: *J. Colloid Interface Sci.*, 1990, vol. 139, pp. 63-86.
12. M. Frenklach and S.J. Harris: *J. Colloid Interface Sci.*, 1987, vol. 118, pp. 252-61.
13. J.J. Wu and R.C. Flagan: *J. Colloid Interface Sci.*, 1988, vol. 123, pp. 339-52.
14. Y. Miki, Y. Shimada, B.G. Thomas, and A. Denissov: *I&SM*, 1997, pp. 31-38.
15. M.J. Hounslow, R.L. Ryall, and V.R. Marshall: *AIChE J.*, 1988, vol. 34, pp. 1821-38.
16. H. Saint-Raymond, F. Gruy, and M. Cournil: *J. Colloid Interface Sci.*, 1998, vol. 202, pp. 238-50.
17. P.G. Saffman and J.S. Turner: *J. Fluid Mech.*, 1956, vol. 1, pp. 16-30.
18. J. Abrahamson: *Chem. Eng. Sci.*, 1975, vol. 30, pp. 1371-79.
19. S. Panchev: *Random Functions and Turbulence*, 1st ed., Pergamon Press, Oxford, United Kingdom, 1971.
20. U. Lindborg and K. Torssell: *Trans. TMS-AIME*, 1968, vol. 242, pp. 94-102.
21. T.A. Engh: *Principles of Metal Refining*, Oxford University Press, New York, NY, 1992, pp. 1-35.
22. A.N. Van and S. Kmet: *Int. J. Miner. Processing*, 1992, vol. 35, pp. 205-23.
23. M. Maniruzzaman and M. Makhlouf: Worcester Polytechnic Institute, Worcester, MA, unpublished research, 2000.
24. J.O. Hinze: *AIChE J.*, 1955, vol. 1, pp. 289-95.
25. S.T. Johansen, S. Gradahl, P. Tetlie, B. Rasch, and E. Myrobstad: *Light Met.*, 1998, pp. 805-10.
26. S.T. Johansen, R. Anvar, and B. Rasch: *Light Met.*, 1999.
27. F.M. White: *Fluid Mechanics*, 3rd ed., McGraw-Hill, Inc., New York, NY, 1994, pp. 487-88.
28. M. Maniruzzaman and M. Makhlouf: *Light Met.*, 1998, pp. 797-803.
29. E.E. Underwood: *Quantitative Stereology*, Addison-Wesley Publishing Company, Reading, MA, 1970.